GEOPHYSICAL RESEARCH LETTERS, VOL. 34, L19501, doi:10.1029/2007GL031204, 2007

Baffin Bay ice drift and export: 2002–2007

Ron Kwok[1]

Received 2 July 2007; revised 14 August 2007; accepted 28 August 2007; published 2 October 2007.

[1] Multiyear estimates of sea ice drift in Baffin Bay and Davis Strait are derived for the first time from the 89 GHz channel of the AMSR-E instrument. Uncertainties in the drift estimates, assessed with Envisat ice motion, are ~2–3 km/day. A persistent atmospheric trough, between the coast of Greenland and Baffin Island, drives the prevailing southward drift pattern with average daily displacements in excess of 18–20 km during winter. Over the 5-year record, the ice export ranges between 360 and 675 $\times$ 10^3 km^2, with an average of 530 $\times$ 10^3 km^2. Sea ice area inflow from the Nares Strait, Lancaster Sound and Jones Sound potentially contribute up to a third of the net area outflow while ice production at the North Water Polynya contributes the balance. Rough estimates of annual volume export give ~500–800 km^3. Comparatively, these are ~70% and ~30% of the annual area and volume exports at the Fram Strait. **Citation:** Kwok, R. (2007), Baffin Bay ice drift and export: 2002–2007, *Geophys. Res. Lett.*, *34*, L19501, doi:10.1029/2007GL031204.

1. Introduction

[2] Baffin Bay, north of Davis Strait, covers an area of ~630 $\times$ 10^3 km^2 and is bounded by Baffin Island in the west, Greenland in the east, and Ellesmere Island in the north. The bay has a width varying between 110 and 650 km. It connects to the Arctic Ocean through the Nares Strait and the straits and channels of the Canadian Arctic Archipelago (CAA). To the south, it is open to the Labrador Sea and the North Atlantic through Davis Strait, the narrowest part of which is ~350 km wide.

[3] The mean circulation pattern of Baffin Bay features a southward flowing cold and fresher Baffin Current along the coast of Ellesmere and a northward flowing West Greenland Current (WGC) along the Greenland coast that brings warm and saltier water from the North Atlantic, with net inflows of Arctic waters and sea ice from the Nares Strait, Lancaster Sound, and Jones Sound. This Arctic water is partly of Pacific origin; it enters the Arctic Ocean through the Bering Strait and then Baffin Bay through the Canadian Arctic Archipelago [*Jones et al.*, 2003]. Baffin Bay serves as the pathway of the fresh and cold Arctic water and sea ice to the Labrador Sea - one of the deep convection sites in the Northern Hemisphere. The mixing, freezing, and melting processes add to the transformation of this water mass. Anomalies in the input of freshwater from Baffin Bay are expected to have consequences in the strength of the meridional overturning circulation [*Goosse et al.*, 1997]; increases in freshwater input from Baffin Bay freshens the upper ocean, stabilizes the water column, and thus weakens convection. A recent study by *Zweng and Münchow* [2006] reports that areas of Baffin Bay associated with the WGC are warming with a likely freshening of surface waters along Baffin Island south of 76°N.

[4] The sea ice of Baffin Bay, whether of Arctic origin or formed locally, represents one component of the freshwater input into the Labrador Sea. The present note addresses this component with a 5-year record daily ice drift in Baffin from the 89 GHz channel of the Advanced Microwave Scanning Radiometer (AMSR-E). With the ice drift fields and other datasets, we examine the seasonal and interannual variability of sea ice circulation within the Bay and the contribution of locally formed sea ice to the total area and volume outflows.

2. Data Description

[5] The primary data sets include: 1) daily ice concentration estimates and gridded 89 GHz brightness temperature (T_b) fields from AMSR-E radiometer on the NASA Aqua platform; 2) Envisat wide-swath Synthetic Aperture Radar (SAR) data; and 3) daily sea level pressure from the NCEP-NCAR analysis products.

2.1. Ice Drift From AMSR-E

[6] Daily ice motion from the 89 GHz T_b fields is obtained using a tracking procedure described by *Kwok et al.* [1998]. The derived fields span a period of ~5 winters (November through May) from 2002 to 2007. The AMSR-E 89 GHz radiometer has a spatial resolution of ~6 km, a twofold improvement over the lower resolution (~12 km) 85 GHz channel on the Special Sensor Microwave Imager (SSM/I) instrument. This added resolution allows us to observe ice drift in smaller regions and narrower channels and straits with reduced uncertainty. Our comparison of the daily motion estimates with 4 years of buoy drift in the Arctic Ocean from the International Arctic Buoy Program (IABP) shows displacement differences with near zero means and standard deviations <~3 km, and directional differences with standard deviations <~20°. The details of this comparison are not discussed here. This can be contrasted to the higher uncertainties of ~5 km and 30° of the 85 GHz data [*Kwok et al.*, 1998].

2.2. Assessment With Envisat SAR Ice Motion

[7] The buoy comparisons are, however, limited to parts of the Arctic with thick multiyear ice where buoys are typically deployed. To assess the quality of the AMSR-E ice motion in the predominantly seasonal ice cover of Baffin Bay, we use a smaller volume of ice motion derived from high-resolution (~100 m) Envisat wide-swath (~450 km) data. Figure 1a shows a 1400 km long Envisat image strip

[1]Jet Propulsion Laboratory, California Institute of Technology, Pasadena, California, USA.

0094-8276/07/2007GL031204$05.00

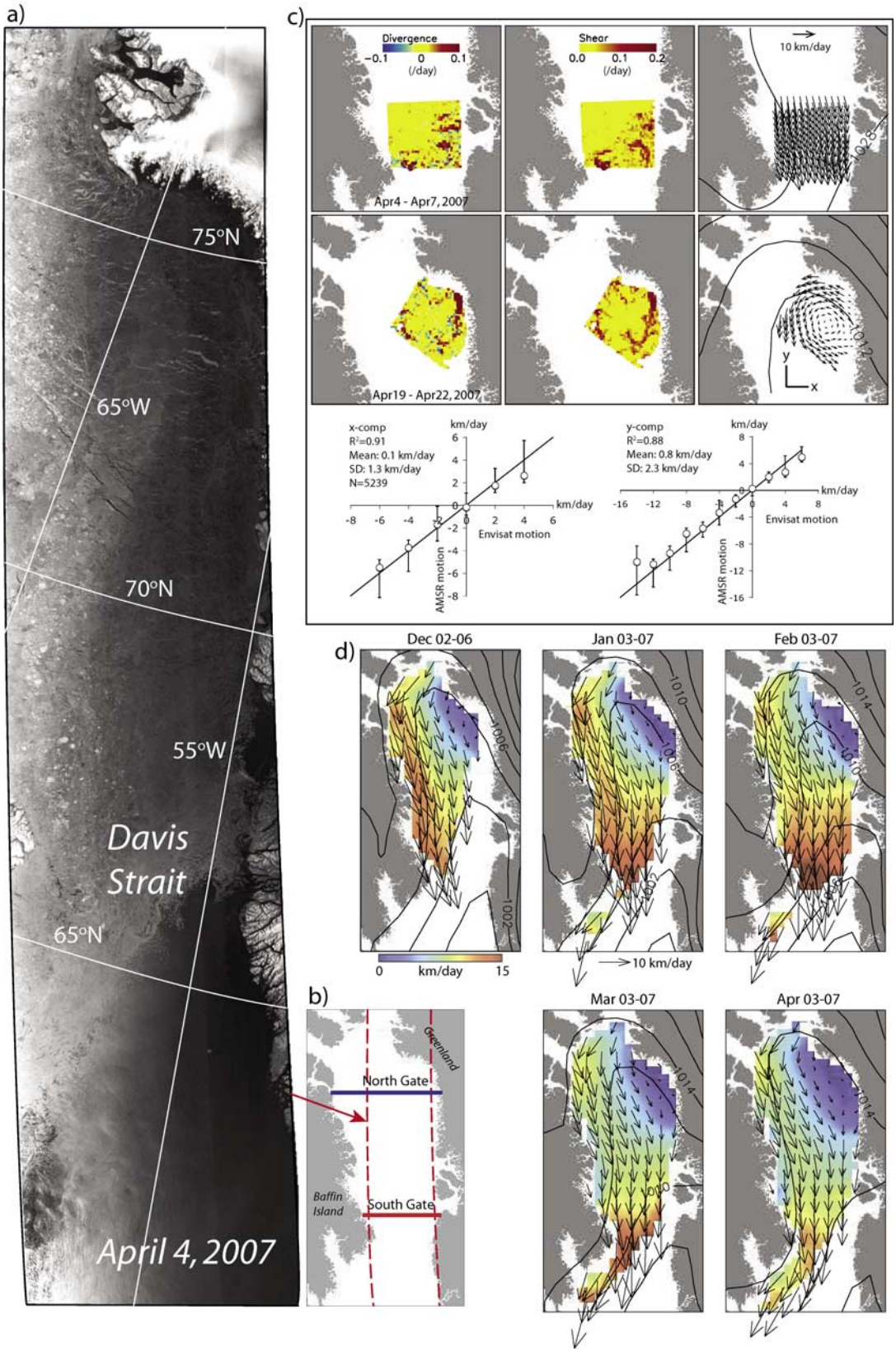

Figure 1. (a) Envisat wide-swath SAR image of Baffin Bay and Davis Strait on April 4, 2007 (Envisat images ©ESA 2007). (b) Map shows the geographic coverage of the Envisat image and the location of the north and south flux gates discussed in the text. (c) Two sample fields of divergence and shear derived from high-resolution Envisat SAR ice drift; comparison of AMSR-E ice motion with Envisat ice motion. (d) Monthly mean ice motion fields (Dec, Jan, Feb, Mar, and Apr) from 2002 through 2007. Isobars of sea level pressure fields, from NCEP, are overlaid on the mean drift. Contour intervals are 2 hPa.

acquired on April 4, 2007 from which some of the ice drift is produced. The image strip covers a large region of Baffin Bay from Smith Sound in the north to the approximate latitude of Godthab in southwest Greenland. The derived Envisat motion estimates, sampled on a high-density (10 km) grid, are visually inspected and erroneous points are discarded. The resulting displacement uncertainties are comparable to that of buoy drift (~300 m) and can be considered to be the reference data set in this case [*Kwok et al.*, 2004]. In total, 5 image pairs with time separations of 2–3 days, acquired in April 2007, are used in this assessment; two examples showing interesting drift patterns (discussed later) are shown in Figure 1c. Prior to the comparisons, the denser Envisat estimates are first degraded spatially to match the spatial resolution of the AMSR-E estimates. Results are shown in the scatterplots of Figure 1c: the standard deviations in the two components of motion (1.3 km/day and 2.3 km/day) are comparable to that observed in the more extensive Arctic Ocean analysis mentioned earlier. The AMSR-E ice motion accounts for close to 90% of the variance in the smoothed Envisat ice motion.

[8] In addition, the high-resolution Envisat kinematics provides a glimpse of the smaller scale strain rates as depicted by the divergence and shear fields shown in Figure 1c. The divergence and shear of each grid cell are computed via: $\nabla \cdot u = u_x + v_y$, $e = [(u_x - v_y)^2 + (u_y + v_x)^2]^{\frac{1}{2}}$. In the equations, u_x, u_y, v_x, v_y are the spatial gradients in ice motion computed using a line integral around the boundary of each 10 km grid cell. The line segments connecting the four vertices define the cell boundaries. $\nabla \cdot u$ is a measure of area change, and e is the scalar magnitude of shear. The first example shows a steady southward drift of sea ice just north of the narrowest portion of the Davis Strait. The maps of these strain measures (in Figure 1c) depict the local deformation of the ice cover. The first example shows significant divergences of up to 0.1/day (red) associated with fractures/openings in a field of relatively undeformed (yellow) ice cover. In the second example, the cyclonic circulation off the west coast of Greenland seems to be a typical feature (as discussed later) in the motion field of Baffin Bay associated with wind, and perhaps current, forcing.

3. Analysis and Discussion

3.1. Ice Drift

[9] Figure 1d shows the mean monthly circulation of sea ice in Baffin Bay from the 5 years of daily ice motion from AMSR-E. The mean southward drift in Baffin Bay, especially in the west, dominates the circulation pattern over all months between November and May. This was also observed in available buoy drift [*Heide-Jørgensen et al.*, 2007].

[10] Sea ice originating in Smith Sound, south of Nares Strait, is typically restricted to the west side of Baffin Bay because of the prevailing drift pattern. This is evident in the backscatter gradient in the Envisat image from April of 2007 (Figure 1a) that is indicative of the relatively higher concentration of multiyear ice in the mix of seasonal and older ice in the western part of the Bay; the higher backscatter ice is from older ice, some of which are characteristic of multiyear ice from the Arctic Ocean. This can be contrasted with the thinner, lower backscatter, seasonal ice in the eastern half of the Bay where almost no signatures of older ice are evident. Across the northern part of the Bay, there is a large gradient in drift speeds (up to 10 km/day) from Baffin Island to the west coast of Greenland. In fact, the ice motion along coastal Greenland, north of 70°N, is predominantly northward. This is associated with a weaker – relative to the motion in the west – cyclonic drift pattern (3–4 km/day). Even though this pattern is not as readily visible in the mean fields, it is clearly illustrated in the Envisat ice drift in Figure 1c. Ice drift is highest in the south: typical ice velocity in winter and early spring is 10 km/day in the southern part of Baffin Bay, increasing to over 20 km/day in Davis Strait with the highest speeds close to Baffin Island.

[11] The seasonal and interannual variability of ice drift at two gates, separated by ~500 km, placed across Baffin Bay are shown in Figures 2a and 2b. The north gate, ~635 km wide (blue in Figure 1b), is positioned at ~73°N while the south gate of ~460 km in width (red in Figure 1b) is positioned at ~68°N. The vector components represent the mean cross-gate (V_x) and along-gate drift (V_y) computed from 3-day averages. Again, prevailing southward motion is seen in the mean drift at both gates at near daily time scales. Only on rare occasions (less than 5% of the time) do the average drift directions reverse. Spatially, the mean southward drift at the north gate is generally smaller than that at the south gate. Mean drift speeds can be >20 km/day. Over the 5-year record, the seasonally averaged $|\overline{V}_y|$ (Nov–May) ranges from 3 km/day to 5.4 km/day at the north gate, and from 6 km/day (04/05) to 8.9 km/day (06/07) at the south gate.

[12] Since atmospheric forcing plays a significant role in sea ice motion, we examine the monthly mean distribution of sea level pressure (SLP). The strength of the circulation also determines the extent and development of the ice cover in Baffin Bay [*Stern and Heide-Jørgensen*, 2003]. Isobars of monthly mean SLP are overlaid on the drift patterns in Figure 1d. There is a persistent trough in SLP between Greenland and Baffin/Ellesmere Islands, the depth of which is highly seasonal. Starting around October, it deepens over the winter but then rapidly weakens during April and May and remains weak throughout the summer. The shape of the trough defines the prevailing geostrophic flow in Baffin Bay that is northwest near the coast of Greenland and southeast in coastal Baffin Island, consistent with the observed ice drift. Using only observations that are more than 100 km from the coast, complex linear regression of the geostrophic wind and ice motion shows that the ice moves with a speed of ~1.3% of the wind, and ~14° to the left of the wind (contrary to the expected right turning of the ice drift due to Coriolis). The wind accounts for ~50% of the variance of the AMSR-E ice drift. The left turning tendencies of the ice drift is perhaps not unexpected. In the Arctic Ocean the effect of the coastline is felt within ~400 km from the coast [*Thorndike and Colony*, 1982]. At distances of less than that, the turning angle and correlation deviate from near-free drift and imply that other processes and effects (e.g., currents and orography) in proximity to the coast weaken the expected relationship between the ice velocity and geostrophic wind.

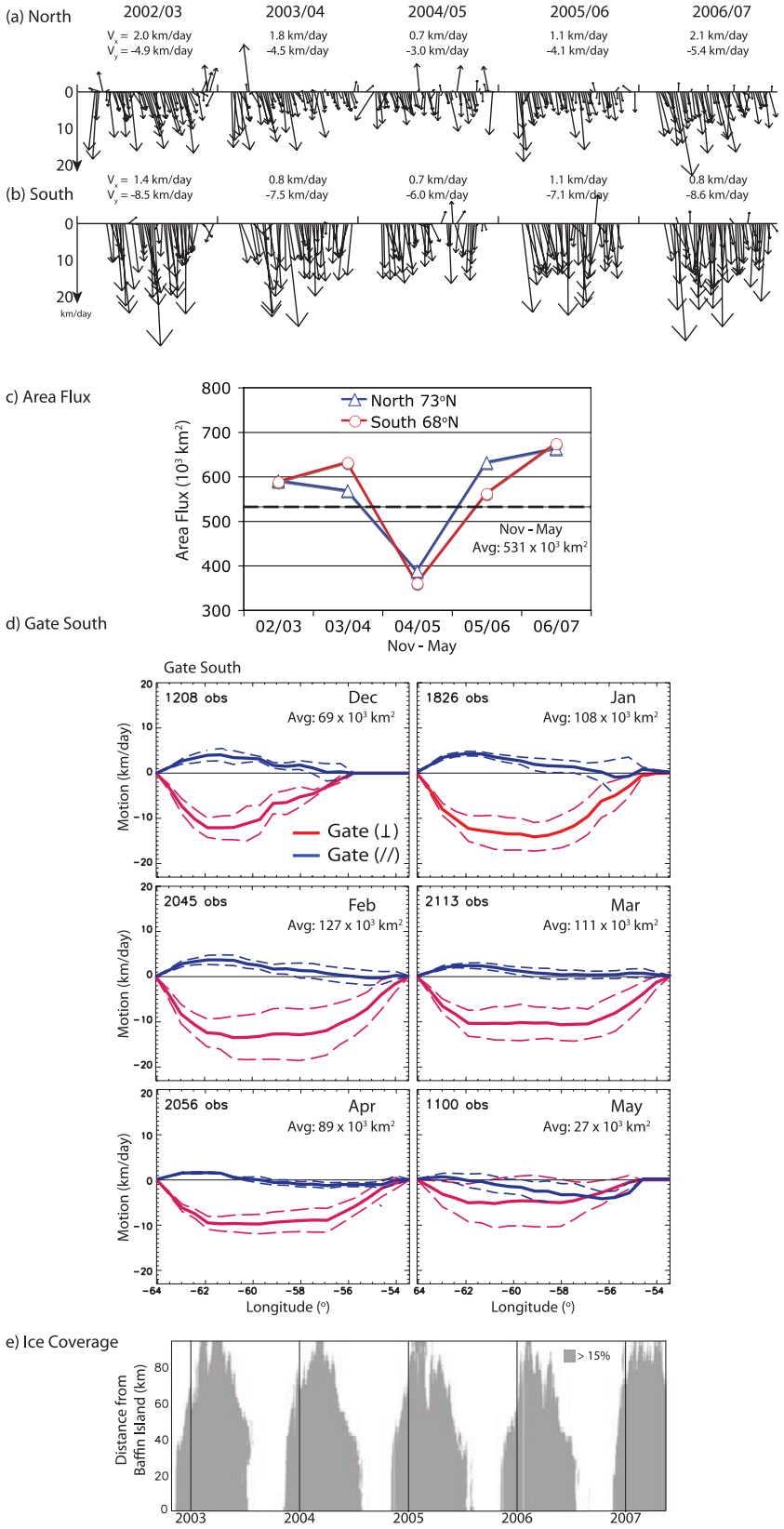

Figure 2. Five winters (November through May) of ice motion, flux, velocity profiles and ice coverage. (a) Gate averaged ice motion – North gate. (b) South gate. (c) Nov-May ice area flux at the north and south gates shown in Figure 1b. (d) Average motion profiles and monthly average area flux at the south gates. (e) Ice coverage along the south gate from 2002 through 2007.

3.2. Ice Area Export

[13] We compute the ice area export at two gates across Baffin Bay described earlier (Figure 1b). The intent is to measure the ice flux near the narrowest stretch of Davis Strait as well as the divergence or area production between the north and south gates.

[14] To compute the daily area flux, the gridded ice motion is first interpolated to the gate and then the gate-perpendicular component of the ice motion is integrated across the gate using the trapezoidal rule. The motion profile is constrained to go to zero at coastal endpoints. To account for open water areas, the area estimates are weighted by the AMSR-E ice concentration. The uncertainties in the area flux over any given time interval, σ_F, can be computed viz.: $\sigma_F = \sigma_u L \sqrt{\frac{N_d}{N_s}}$ [*Kwock and Rothrock*, 1999]. In this equation: L is the width of the flux gate, σ_u is the standard deviation in the displacement estimates, N_s is the number of independent samples across the gate, and N_d is the number of daily estimates in the record. Using 180 days (i.e. N_d) of data to compute the total winter area flux, $N_s = 10$ at the north gate, $N_s = 7$ at the south gate, and $\sigma_u = 3$ km, give uncertainties of 8000 km^2 and 6500 km^2 in their total winter area flux.

[15] Figure 2c shows the five years (2002–2007) of ice area export at the two gates. For the 5-year winter record (02/03, 03/04, 04/05, 05/06, and 06/07) the Nov–May ice area flux at the south gate are: 590, 630, 360, 560 and 675 $\times$ 10^3 km^2, with an average of 530 $\times$ 10^3 km^2. The overall uncertainties computed above are small compared to the size of the annual area flux. This average area flux is over 70% of the average winter area export at Fram Strait of $\sim$750 $\times$ 10^3 km^2. During two of the five winters, Baffin Bay exported up to its own area ($\sim$690 $\times$ 10^3 km^2) of sea ice. The high and low area flux years, 2004/05 and 2006/07, can be seen in the differences between the average cross gate ice motion for the two years (Figures 2a and 2b) at both gates. At the south gate, the average southward drift speed, over the winter is 6 km/day during the low year and 8.6 km/day in the high year.

[16] The mean (solid line) and standard deviation (dashed lines) of the monthly gate profiles for the 5 years is shown in Figure 2d. The gate-perpendicular profile shows the largest outflow in the western part of the gate; the peak of the profile is centered slightly east of 82°W. Along the gate, the dominant eastward advection of ice can be seen in the gate-parallel ($\|$) profile with a peak skewed even more toward western Baffin Bay. Due to the prevailing southward drift, the magnitudes of the gate perpendicular motion are generally several times greater than gate parallel motion. Seasonally, the largest outflow at the south gate is in February. The annual ice coverage of the south gate is shown in Figure 2e: this part of Davis Strait is generally ice-free between June and September; the coverage advances rapidly from west to east in November with maximum coverage attained in the late winter with the ice edge occasionally reaching the west coast of Greenland; the retreat westward starts around March. The lower ice coverage in the east is likely associated with southerly circulation and the warm West Greenland Current.

[17] The differences in area flux between the two gates (south minus north) are: 0, 60, −30, −70, and 11 $\times$ 10^3 km^2. The ice flux through the wider north gate (635 km) and narrower south gate (460 km) are comparable and balanced by the higher ice velocity at the south gate (Figure 2c). Unless there is significant ice convergence, these small differences in area flux indicate that the ice area production is relatively small (compared to the net flux) in that part of Baffin Bay between the two gates. This also suggests that most of the ice area is produced in Baffin Bay north of $\sim$73°N.

[18] There are three sources of ice area in northern Baffin Bay: inflow from the Arctic Ocean and the Canadian Arctic Archipelago (CAA); ice production in the North Water polynyas; and local ice divergence/convergence. The first source is associated with inflows of sea ice of Arctic- and CAA-origin through the Nares Strait, Lancaster Sound, and Jones Sound. *Kwok* [2005] estimates an annual ice flux of 33 $\times$ 10^3 km^2 of primarily thick Arctic multiyear (MY) sea ice into Nares Strait through a gate positioned at Robeson Channel just south of the Lincoln Sea. Seasonally, this ice flux from the Arctic is most active after July and ceases after the formation of an ice bridge in mid- to late-winter, and recommences after breakup in late spring and early summer. Overall, this inflow contributes only a small fraction to the total ice area flux at the north gate. Even though this is a relatively small areal contribution to the net flux, this thick Arctic MY ice contributes (discussed later) to the total volume outflow. In the absence of a winter ice bridge at Nares Strait, the inflow of Arctic Ocean ice could be potentially higher. The contribution of sea ice inflow from Lancaster Sound and Jones Sound to the Baffin Bay outflow is not as well known. According to a recent study [*Kwok*, 2006], there is very little exchange of sea ice between the CAA and the Arctic Ocean; thus this sea ice is most likely produced within the CAA. Rough estimates from the mid-1970s provided by *Dey* [1981] give average annual inflows of 170 $\times$ 10^3 km^2 (Lancaster) and 20 $\times$ 10^3 km^2 (Jones). These earlier results are based on general estimates of ice motion and thickness derived from coarse satellite imagery, reconnaissance flight, ship observations and field programs. Unfortunately, these are rough estimates and the uncertainties are not quantified. Taking the sum of these quantities, the Lancaster and Jones Sound inflow could account for a third of the Baffin Bay ice outflow of 530 $\times$ 10^3 km^2.

[19] Significant ice production in northern Baffin Bay is associated with one of the largest recurring polynyas in the Arctic, the North Water (NOW) Polynya [*Ingram et al.*, 2002]. Strong northerly winds create the conditions necessary to maintain this polynya where newly-formed ice is swept southward under the combined effects of wind and currents. In one study of the ice motion in the NOW region, *Wilson et al.* [2001] report that large areas of sea ice originate from the polynya. However, we are not aware of any quantitative estimates of its winter ice area production in the published literature. Using the estimated Arctic and CAA inflows from above and the ice flux at the north gate allows a rough estimate of the ice area production at the NOW polynya. Subtracting the sea ice inflows and neglecting the contributions due to ice deformation in the consolidated ice cover, we obtain an annual area production of $\sim$300 $\times$ 10^3 km^2 or about two-thirds of the ice area flux.

This suggests that the NOW polynya is the dominant region of ice production in Baffin Bay.

[20] As for ice area production due to deformation, openings and closings add to and take away from total ice area. Since the Baffin Bay is only a semi-enclosed sea unconstrained by land boundaries to the south, we expect the ice cover to be net divergent but this remains to be demonstrated with higher quality motion data with better spatial and temporal resolutions.

3.3. Rough Estimate of Volume Export

[21] With the above estimate of ice area flux, we can make a preliminary estimate of the ice volume flux through the Davis Strait. However, available sea ice thickness measurements from Baffin Bay are limited. Based on published literature, *Tang et al.* [2004] summarized the ice thickness synthesized from a variety of sources: in-situ measurements, interpretation of satellite imagery, and model simulations. Briefly, the Baffin Bay ice cover is mostly seasonal with a small amount of multiyear ice inflow from the Nares Strait and Lancaster Sound. Due to the drift pattern, the multiyear ice distribution is largely restricted to western Baffin Bay. Seasonal ice formed in the fall can attain a thickness of 1.2 m and seems to be the dominant ice thickness. The western side of the pack ice contains hummocky floes and floes that are extremely rough and laced with pressure ridges exceeding 3 m. The mean thickness of level ice decreased from 1.75 m in the northwest, to less than 0.75 m in the southeast. Along the coast of Baffin Island, the mean thickness tends to be in the range of 1.25–1.5 m. Summarizing, there is a thickness gradient across the Davis Strait with thicker, more deformed ice (1–2 m) in the west and thinner ice (<1 m) in the east. Since the ice cover is seasonal, we also expect the ice cover to gradually increase in thickness over the winter due to ice growth. Taking the annual average ice thickness at the south gate to be 1–1.5 m and an average ice area flux of 530×10^3 km^2, we obtain an ice volume flux of 530–800 km^3. This can be compared to the work of *Cuny et al.* [2005], who gave an estimate of ~500 km^3 using coarser SSM/I ice drift and assuming an average thickness of 1 m. Of this total volume, ~100 km^3 could be due to multiyear ice inflow from the Nares Strait [*Kwok*, 2005]. These results suggest that the average volume export is a third of the sea ice outflow at the Fram Strait of ~2200 km^3 [*Kwok et al.*, 2004].

4. Conclusions

[22] The present note examines the ice drift in Baffin Bay using a 5-year record (2002–2007) derived from the 89 GHz channel of the AMSR-E instrument on the NASA Aqua platform. The ~6 km spatial resolution of AMSR-E represents a twofold improvement over that of the 85 GHz channel on the SSM/I instrument. Although not of sufficient quality for examining small-scale deformation, this improved resolution allows us to observe ice drift in smaller regions, and narrower channels and straits with reduced uncertainty. Uncertainties in the daily drift estimates in Baffin Bay, assessed with Envisat ice motion, at ~2–3 km/day, are consistent with that observed in the Arctic Ocean. With AMSR-E, systematic monitoring of the daily ice drift in Baffin Bay is now possible. The prevailing southward drift in Baffin Bay has average daily displacements of up to 18–20 km in winter, especially in the south. A persistent atmospheric trough of seasonally varying depth, between the coast of Greenland and Baffin Island, drives the ice motion. A mix of first-year and multiyear sea ice can be seen in available Envisat SAR imagery. Multiyear ice from the Nares Strait and the CAA are however restricted to the western side of the Bay because of the drift pattern.

[23] For the 5-year winter record (02/03, 03/04, 04/05, 05/06, and 06/07) the Nov–May ice area flux at the south gate are: 590, 630, 360, 560 and 675×10^3 km^2, with an average of 530×10^3 km^2. While the interannual variability seems significant, this is a very short record of ice drift analysis and ice area export estimates and may not be typical of long-term behavior. Estimates of sea ice area inflow from the Nares Strait, Lancaster Sound and Jones Sound suggest that these sources could contribute potentially up to a third of the net outflow. Ice production at the North Water Polynya is significant, possibly accounting for the other two-thirds.

[24] Rough estimates of annual volume export give a value of ~500–800 km^3 (12 –19 mSv); this is an order of magnitude smaller than the liquid component of ~100 mSv [*Cuny et al.*, 2005]. Comparatively, these annual area and volume exports are ~70% and ~30% of that at the Fram Strait. With relatively good quality ice motion from AMSR-E, the uncertainty in sea ice thickness is the largest source of error in the estimation of volume flux. This again underscores the need for sea ice thickness measurements from either moored upward looking sonars or satellite measurements for refining these estimates in the future.

[25] **Acknowledgments.** I wish to thank S. S. Pang for her assistance during the preparation of this manuscript. The AMSR-E brightness temperature and ice concentration fields were provided by World Data Center A for Glaciology/National Snow and Ice Data Center, University of Colorado, Boulder, CO. This work was performed at the Jet Propulsion Laboratory, California Institute of Technology and is sponsored by the National Science Foundation and the National Aeronautics and Space Administration.

References

Cuny, J., P. Rhines, and R. Kwok (2005), Davis Strait fluxes, *Deep Sea Res., Part I*, *52*, 519–542.

Dey, B. (1981), Monitoring winter sea ice dynamics in the Canadian Arctic with NOAA-TIR images, *J. Geophys. Res.*, *86*, 3223–3235.

Goosse, H., T. Fichefet, and J.-M. Campin (1997), The effects of the water flow through the Canadian Archipelago in a global ice-ocean model, *Geophys. Res. Lett.*, *24*, 1507–1510.

Heide-Jørgensen, M. P., H. Stern, and K. Laidre (2007), Dynamics of the sea ice edge in Davis Strait, *J. Mar. Syst.*, *67*, 170–178, doi:10.1016/j.jmarsys.2006.10.011.

Ingram, R. G., J. Bâcle, D. G. Barber, Y. Gratton, and H. Melling (2002), An overview of physical processes in the North Water, *Deep Sea Res., Part II*, *49*, 2893–4906.

Jones, E. P., J. H. Swift, L. G. Anderson, M. Lipizer, G. Civitarese, K. K. Falkner, G. Kattner, and F. McLaughlin (2003), Tracing Pacific water in the North Atlantic Ocean, *J. Geophys. Res.*, *108*(C4), 3116, doi:10.1029/2001JC001141.

Kwok, R. (2005), Variability of Nares Strait ice flux, *Geophys. Res. Lett.*, *32*, L24502, doi:10.1029/2005GL024768.

Kwok, R. (2006), Exchange of sea ice between the Arctic Ocean and the Canadian Arctic Archipelago, *Geophys. Res. Lett.*, *33*, L16501, doi:10.1029/2006GL027094.

Kwock, R., and D. A. Rothrock (1999), Variability of Fram Strait Flux and North Atlantic Oscillation, *J. Geophys. Res.*, *104*, 5177–5189.

Kwok, R., A. Schweiger, D. A. Rothrock, S. Pang, and C. Kottmeier (1998), Sea ice motion from satellite passive microwave imagery assessed with ERS SAR and buoy motions, *J. Geophys. Res.*, *103*, 8191–8214.

Kwok, R., G. F. Cunningham, and S. S. Pang (2004), Fram Strait sea ice outflow, *J. Geophys. Res.*, *109*, C01009, doi:10.1029/2003JC001785.

Stern, H. L., and M. P. Heide-Jørgensen (2003), Trends and variability of sea ice in Baffin Bay and Davis Strait, 1953–2001, *Polar Res.*, *22*, 11–18.

Tang, C. L., C. K. Ross, T. Yao, B. Petrie, B. M. DeTracy, and E. Dunlop (2004), The circulation water masses and sea ice of Baffin Bay, *Prog. Oceanogr.*, *63*, 183–228.

Thorndike, A. S., and R. Colony (1982), Sea ice motion in response to geostrophic winds, *J. Geophys. Res.*, *87*, 5845–5852.

Wilson, K., D. G. Barber, and D. J. King (2001), Validation and production of RADARSAT-1 derived ice-motion maps in the North Water (NOW) Polynya, January–December 1988, *Atmos. Ocean*, *39*, 257–278.

Zweng, M. M., and A. Münchow (2006), Warming and freshening of Baffin Bay, 1916–2003, *J. Geophys. Res.*, *111*, C07016, doi:10.1029/2005JC003093.

R. Kwok, Jet Propulsion Laboratory, California Institute of Technology, 4800 Oak Grove Drive, Pasadena, CA 91109, USA. (ron.kwok@jpl.nasa.gov)